ISSN 0023-1584, Kinetics and Catalysis, 2007, Vol. 48, No. 2, pp. 255–264. © MAIK "Nauka/Interperiodica" (Russia), 2007.
Original Russian Text © Yu.A. Agafonov, N.V. Nekrasov, N.A. Gaidai, A.L. Lapidus, 2007, published in Kinetika i Kataliz, 2007, Vol. 48, No. 2, pp. 271–280.

Kinetics and Mechanism of the Oxidative Dehydrogenation of Isobutane on Cobalt, Nickel, and Manganese Molybdates

Yu. A. Agafonov, N. V. Nekrasov, N. A. Gaidai, and A. L. Lapidus

Zelinskii Institute of Organic Chemistry, Russian Academy of Sciences, Moscow, 119991 Russia

e-mail: gaidai@ioc.ac.ru

Received April 14, 2005

Abstract—The kinetics of oxidative dehydrogenation of isobutane in the presence of atmospheric oxygen on manganese molybdate has been studied. The experiments have been carried out in a circulation flow reactor at 470–530°C. The form of kinetic equations and the mechanism of the formation of isobutene, carbon oxides, and cracking products on manganese molybdate are similar to those found previously for the same reaction on cobalt and nickel molybdates. The highest yields of isobutene and propene (isobutane cracking products) are achieved on $Co_{0.95}MoO_4$. The mechanism of the process has been investigated by the unsteady-state response method. Manganese molybdate contains the largest amount of reactive oxygen, whereas nickel molybdate contains the smallest amount of reactive oxygen. The earlier conclusion that molybdate lattice oxygen and chemisorbed oxygen play the main role in the formation of *iso*-C_4H_8 and in deep oxidation processes, respectively, is confirmed.

DOI: 10.1134/S0023158407020097

INTRODUCTION

The demand for olefins, including isobutene, which is used in the synthesis of various organic products (polybutylenes, alkylates, copolymers, methyl *tert*-butyl ether, etc.), is steadily increasing. A promising method of olefin production is the oxidative dehydrogenation of paraffins. This process requires much less energy than simple dehydrogenation or cracking. Furthermore, the oxidant involved in the reaction considerably hampers coke formation, a process that can cause both a loss of raw materials and catalyst deactivation.

Various systems, including simple and multicomponent oxides, oxychlorides, zeolites, borates, heteropolyacids, noble metals, etc., can serve as catalysts for the oxidative dehydrogenation of lower paraffins [1–4]. The reports concerning oxidative dehydrogenation have mainly been devoted to selection of catalysts for this process. Different vanadium-based oxide systems are most often considered as catalysts for the oxidative dehydrogenation of light paraffins. Molybdenum oxide catalysts exceeding vanadium systems in olefin selectivity in some cases have recently been studied. In particular, nickel, magnesium, and cobalt molybdates are efficient catalysts for the oxidative dehydrogenation of lower paraffins [5–24].

The kinetic studies of oxidative dehydrogenation on these catalysts were carried out using reactions involving propane [23, 24] and *n*-butane [10, 12]. The rate of propane oxidative dehydrogenation on β-$NiMO_4$ was described in terms of a power-law equation first-order with respect to propane and zero-order with respect to oxygen [23]. The mechanism proposed for this process [23] assumes the presence of three distinct types of adsorption sites for propene, oxygen, and water. Propane adsorption or the interaction between adsorbed propane and lattice oxygen is considered to be the slowest step of the process. The same power-law equation was suggested for propane oxidative dehydrogenation on nickel molybdate (α- and β-phases) [24].

A series of works have been devoted to *n*-butane oxidative dehydrogenation on nickel α- and β-molybdates, either unpromoted or promoted with an alkali metal (Li, Na, K, and Cs) [5, 7, 9–14]. Nickel α-molybdate has a higher activity than the β-phase, but the C_4 olefin selectivity is much higher on the latter at the same conversion and temperature [9]. Power-law equations were obtained for the formation rate of butenes and carbon oxides in *n*-butane oxidative dehydrogenation on nickel molybdate catalysts promoted with alkali metals [10, 12]. On both the unpromoted and promoted catalysts, the reaction order with respect to *n*-butane is close to unity and reaction order with respect to oxygen is close to zero. The oxidative dehydrogenation is considered [5, 7, 9–14] to proceed via the Mars–Van Crevelen redox mechanism. This mechanism is most often used to describe the oxidative dehydrogenation of paraffins in the presence of oxides of metals that easily change their oxidation state (V, Mo, W, etc.).

The use of unsteady-state methods in the study of the oxidative dehydrogenation of lower paraffins has received insufficient attention, although these methods can provide valuable mechanistic information [25–27]. Experiments using an alternating supply of propane and oxygen to nickel molybdate (with intermediate

purging of the system with He) demonstrated that lattice oxygen is involved in propene formation [24]; that is, the reaction proceeds via the Mars–Van Crevelen mechanism. Transient processes were also used to study the mechanism of propane oxidative dehydrogenation on vanadium catalysts [28, 29].

As follows from the literature, gradientless methods have not been employed up to now in kinetic studies of the oxidative dehydrogenation of light paraffins. The mechanism of the oxidative dehydrogenation of paraffins under unsteady-state conditions has been addressed very rarely, and most of the relevant studies have been limited to propane dehydrogenation.

Earlier, we studied the kinetics and mechanism of isobutane oxidative dehydrogenation on cobalt and nickel molybdates [30]. Here, we report the kinetics of isobutane oxidative dehydrogenation on manganese molybdate, transient processes, and the effect of the reaction medium on the reaction in the presence of cobalt, nickel, and manganese molybdates. Furthermore, we compare the activities and selectivities of the catalysts.

EXPERIMENTAL

The catalysts $NiMO_4$, $Co_{0.95}MoO_4$, and $MnMoO_4$[1] were prepared by coprecipitation from aqueous solutions of respective metal nitrates and ammonium molybdate using a standard procedure [31]. Their BET specific surface areas were 32, 23, and 2.5 m^2/g, respectively. As was demonstrated in earlier works (see, e.g., [21, 22]), the addition of molybdenum oxide (1 to 10%) to nickel, magnesium, or cobalt molybdate produces a favorable effect. For this reason, a 5% excess of MoO_3 was introduced into the cobalt–molybdenum catalyst. The introduction of this small stoichiometric excess of Mo results in a noticeable increase in the reaction selectivity with respect to the oxidative dehydrogenation products of light paraffins.

Kinetic experiments were carried in a one-piece glass gradientless flow circulating reactor under atmospheric pressure. The reaction mixture was analyzed by gas chromatography using two columns. Isobutane, isobutene, cracking products, and carbon dioxide were identified on the first column, which was packed with Chromaton supporting 20% triethylene glycol *n*-butyrate. The second column, packed with molecular sieve 5 Å, was used to identify oxygen, nitrogen, and carbon oxide.

Before the experiments, the catalysts were treated with flowing air at 550°C for 2 h. The reactor was charged with 0.2–0.4 g of a catalyst with a particle size of 0.25–0.5 mm.

[1] These catalysts were kindly presented by M. Portela (CRECAT, Instituto Superior Tecnico, Lisbon, Portugal), V. Corberan (Instituto de Catalysis y Petroleoquimica, CSIC, Madrid, Spain), and F. Trifiro (Universita di Bologna, Italy).

At a constant flow rate and invariable initial concentrations of isobutane and oxygen, the rate of accumulation of the reaction products on $MnMoO_4$ at 530°C was independent of the circulation rate; i.e., the process was not controlled by external diffusion. The rate of the reaction on the $MnMoO_4$ particles smaller than 1 mm in diameter was independent of the catalyst particle size; i.e., there were no internal diffusion limitations and the process was kinetically controlled.

The catalyst was placed between quartz layers to prevent any substantial contribution from homogeneous reactions. In the reactor filled with quartz alone, the isobutane conversion was about 3% at 550°C and the lowest flow rate of the reaction mixture (3 l/h). This contribution from homogeneous reactions can be considered insignificant.

Transient processes were studied by the response method [25–27], monitoring how a sharp change in the concentration of one or both components of the reaction affects the state of the system. The experiments were carried out in a small-volume reactor connected to an MSKh-6 time-of-flight mass spectrometer. This made it possible to determine the composition of the reaction mixture directly during comparatively fast relaxation processes. The residence time (i.e., the ratio of the reactor volume to the flow rate) did not exceed 4 s. This time was taken into account when plotting the relaxation curves. In all runs, the relaxation time derived from response curves was shorter than the reaction turnover time. The fulfillment of this condition was among the main features that allowed us to assign the observed relaxations to inherent processes [32], associated with the reaction mechanism rather than with side processes. Peaks with mass numbers 15 (methane), 18 (water), 32 (oxygen), 43 (isobutane), 44 (carbon dioxide), and 56 (isobutene) were monitored during mass spectrometric analysis. The effect of the reaction mixture was studied in the same apparatus as the transient processes.

RESULTS AND DISCUSSION

Kinetics of Isobutane Oxidative Dehydrogenation on Manganese Molybdate under Stationary Conditions

The kinetics of isobutane oxidative dehydrogenation on $MnMoO_4$ was studied at 470 to 530°C, isobutane partial pressures of $P^0_{C_4H_{10}}$ = 0.10–0.35 atm, oxygen partial pressures of $P^0_{O_2}$ = 0.015–0.20 atm, and reaction mixture flow rates of 5000–40000 h^{-1}. Under these conditions, the isobutane conversion (X) ranged between 0.02 and 0.27 and the olefin selectivity (S) ranged between 0.50 and 0.97. The major reaction products were isobutene, cracking products (methane and propene), carbon oxides, and water.

The curve that describes the dependence of the concentration of the resulting CO_2 on the isobutane conversion (Fig. 1) is concave; i.e., the CO_2 formation rate

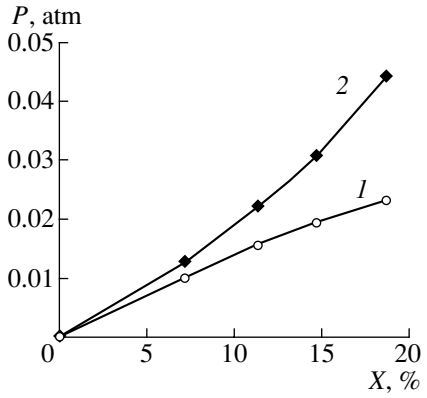

Fig. 1. Partial pressures of resulting (*1*) *iso*-C_4H_8 and (*2*) CO_2 versus isobutane conversion on $MnMoO_4$ at 500°C.

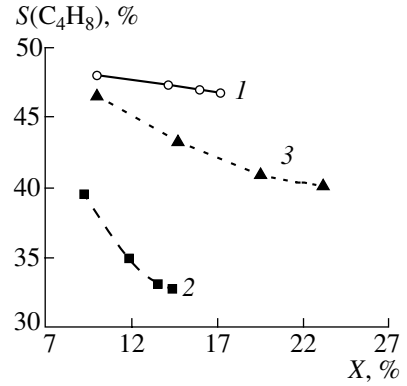

Fig. 2. *iso*-C_4H_8 formation selectivity versus isobutane conversion on (*1*) $Co_{0.95}MoO_4$, (*2*) $NiMoO_4$, and (*3*) $MnMoO_4$ at 530°C.

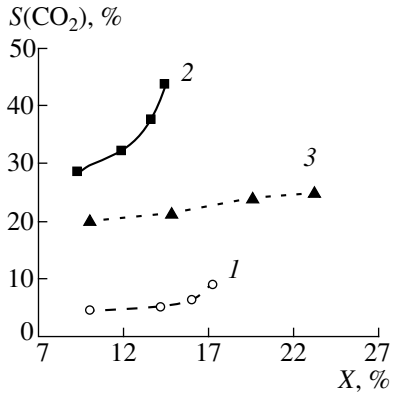

Fig. 3. CO_2 formation selectivity versus isobutane conversion on (*1*) $Co_{0.95}MoO_4$, (*2*) $NiMoO_4$, and (*3*) $MnMoO_4$.

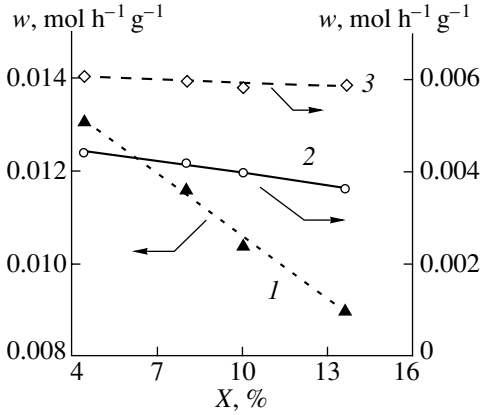

Fig. 4. Accumulation rates of (*1*) *iso*-C_4H_8, (*2*) C_3H_6, and (*3*) CO_2 versus isobutane conversion on $MnMoO_4$ at 470°C.

increases with increasing conversion. This is possible if isobutene is oxidized more rapidly than the initial paraffin. This conclusion is in agreement with the experimental fact that the isobutene accumulation rate decreases as the conversion increases. The rate of CO_2 formation on $Co_{0.95}MoO_4$ and $NiMoO_4$ increases more rapidly with increasing conversion [30]. The amount of CO_2 formed on $MnMoO_4$ is much larger than the amount of the resulting CO, as in the case of the $Co_{0.95}MoO_4$ and $NiMoO_4$ catalysts.

The plots of the *iso*-C_4H_{10} and CO_2 selectivity versus the total isobutane conversion for cobalt, nickel, and manganese molybdates are presented in Figs. 2 and 3. The CO_2 selectivity curves (Fig. 3) for nickel and cobalt molybdates, unlike the same curve for manganese molybdate, are concave. This possibly indicates that olefins that are oxidized first are adsorbed less strongly on the $MnMoO_4$ surface.

As the isobutane conversion approaches zero, the reaction selectivities with respect to CO_2, CO, *iso*-C_4H_{10}, and C_3H_6 do not tend to zero. This implies that these compounds are primary products formed directly from isobutane.

Figure 4 plots the accumulation rates of isobutene and propene resulting from isobutane cracking and the CO_2 formation rate versus the total isobutane conversion on manganese molybdate. The isobutene accumulation rate decreases more rapidly than the propene accumulation rate. This is due to the fact that isobutene, unlike propene, undergoes further transformations. The decrease in the propene accumulation rate is caused by a decrease in the partial pressure of isobutane rather than the oxidation of this olefin. The fact that the CO_2 formation rate changes insignificantly with increasing isobutane conversion is most likely due to the oxidation of isobutene, whose concentration in the reaction mixture increases with an increase in *X*.

Experimental data were processed under the assumption that deep oxidation and cracking proceed via an adsorption mechanism. The reaction orders with respect to hydrocarbons in all processes were accepted to be 1, and the reaction order with respect to oxygen was varied between 0 and 2.0 with an increment of

Table 1. Experimental and calculated (Eqs. (1)–(4)) rates of accumulation of the isobutane oxidative dehydrogenation products on $MnMoO_4$

T, °C	$P_{C_4H_{10}}$, atm	P_{O_2}, atm	$P_{C_4H_8}$, atm	w_i, mol h^{-1} g^{-1}							
				iso-C_4H_8		C_3H_6		CO_2		CO	
				observed	calculated	observed	calculated	observed	calculated	observed	calculated
470	0.216	0.106	0.022	0.0090	0.0111	0.0036	0.0038	0.0059	0.0058	0.0032	0.0034
	0.225	0.112	0.017	0.0103	0.0119	0.0040	0.0039	0.0058	0.0059	0.0033	0.0035
	0.230	0.121	0.014	0.0116	0.0127	0.0042	0.0039	0.0060	0.0060	0.0034	0.0035
	0.239	0.131	0.008	0.0131	0.0138	0.0044	0.0040	0.0061	0.0061	0.0036	0.0036
500	0.198	0.086	0.027	0.0098	0.0118	0.0050	0.0051	0.0172	0.0175	0.0054	0.0053
	0.210	0.107	0.022	0.0116	0.0137	0.0053	0.0052	0.0192	0.0183	0.0055	0.0055
	0.218	0.115	0.018	0.0128	0.0147	0.0051	0.0052	0.0197	0.0187	0.0056	0.0055
	0.230	0.125	0.013	0.0165	0.0161	0.0059	0.0054	0.0210	0.0192	0.0059	0.0056
530	0.179	0.071	0.029	0.0102	0.0128	0.0068	0.0097	0.0255	0.0279	0.0086	0.0090
	0.190	0.075	0.027	0.0132	0.0139	0.0074	0.010	0.0294	0.0283	0.0096	0.0092
	0.202	0.085	0.023	0.0138	0.0162	0.0075	0.010	0.0296	0.0288	0.0093	0.0095
	0.219	0.091	0.018	0.0193	0.0178	0.0097	0.011	0.0322	0.0292	0.0118	0.0098

0.25. When choosing a rate equation, the power of the denominator was taken to be 0, 1, or 2. The rates of formation of the reaction products on manganese molybdate are best described by the following equations, which were set up earlier for cobalt and nickel molybdates [30]:

$$\text{isobutene } r_{\mathrm{I}} = \frac{k_{\mathrm{I}} P_{C_4H_{10}} P_{O_2}}{P_{O_2} + k_1 P_{C_4H_{10}}}, \quad (1)$$

$$\text{carbon dioxide } r_{\mathrm{II}} = \frac{(k_{\mathrm{II}} P_{C_4H_{10}} + k'_{\mathrm{II}} P_{C_4H_8}) P_{O_2}^{0.5}}{P_{O_2}^{0.5} + k_2 (P_{C_4H_8} + P_{C_3H_6})}, \quad (2)$$

carbon monoxide

$$r_{\mathrm{III}} = \frac{(k_{\mathrm{III}} P_{C_4H_{10}} + k'_{\mathrm{III}} P_{C_4H_8}) P_{O_2}^{0.5}}{P_{O_2}^{0.5} + k_2 (P_{C_4H_8} + P_{C_3H_6})}, \quad (3)$$

cracking products

$$r_{\mathrm{IV}} = \frac{k_{\mathrm{IV}} P_{C_4H_{10}}}{P_{O_2}^{0.5} + k_2 (P_{C_4H_8} + P_{C_3H_6})}. \quad (4)$$

In view of the fact that isobutene turns into carbon oxides, the apparent *iso*-C_4H_{10} accumulation rate ($w_{C_4H_8}$) can be expressed in terms of the rate equation

$$w_{C_4H_8} = r_{\mathrm{I}} - \frac{[(k'_{\mathrm{II}} + k'_{\mathrm{III}}) P_{C_4H_8}] P_{O_2}^{0.5}}{P_{O_2}^{0.5} + k_2 (P_{C_4H_8} + P_{C_3H_6})}. \quad (5)$$

A comparison between the accumulation rates determined experimentally and the same rates calculated using rate equations (1)–(4) shows that the calculation error is 14.5% for an experimental error of 10.3% (Table 1). Attempts to fit the experimental isobutene accumulation rates to other equations, including power-law equations and the Langmuir–Hinshelwood equation, resulted in errors larger than are observed with Eq. (5).

The physical meaning of the constants in Eq. (1) will be clear from the further discussion. The numerators of Eqs. (2)–(5) contain the constants k_{II}, k'_{II}, k_{III}, k'_{III}, and k_{IV}, which involve the rate constants of the corresponding slow steps; the constant k_2 in the denominators of these equations is the ratio of the adsorption constants of the olefins (C_4H_8 and C_3H_6) and oxygen. The following conclusions can be drawn from the comparison of the constants in Eqs. (1)–(4) (Table 2):

(1) The rate of isobutene formation is the highest on the nickel molybdate (compare k_{I} values).

(2) Nickel molybdate is the most active catalyst in the oxidation of both the initial paraffin and isobutene (compare the constants k_{II}, k'_{II}, k_{III}, and k'_{III}).

(3) Olefins are bound least strongly by the manganese molybdate surface and most strongly by nickel molybdate (compare the values of the adsorption constant k_2).

Transient Processes in the Oxidative Dehydrogenation of Isobutane

The transient processes were studied using the response method [26, 27] by monitoring the changes in the concentrations of the reaction components (until the steady state was reached) as the response to a sharp change in the feed composition. The shape and length of the relaxation curves provide information concern-

Table 2. Constants of rate equations (1)–(4) describing isobutane conversion on $Co_{0.95}MoO_4$, $NiMoO_4$, and $MnMoO_4$

Catalyst	T, °C	Constant							
		k_1	k_I	k_{II}	k'_{II}	k_{III}	k'_{III}	k_{IV}	k_2, $atm^{-0.5}$
			mol g^{-1} h^{-1} atm^{-1}						
$Co_{0.95}MoO_4$	480	0.72	0.17	0.0064	0.026	0.0039	0.017	0.0093	6.1
	500	0.65	0.23	0.0090	0.035	0.0054	0.023	0.018	5.2
	530	0.60	0.30	0.012	0.046	0.0075	0.034	0.034	4.0
	550	0.56	0.34	0.014	0.054	0.0092	0.043	0.049	3.7
$NiMoO_4$	500	2.2	0.29	0.076	0.30	0.018	0.072	0.0064	26
	530	1.9	0.55	0.10	0.40	0.033	0.13	0.015	13
	550	1.7	0.61	0.13	0.49	0.049	0.20	0.026	6.4
$MnMoO_4$	470	1.6	0.23	0.0062	0.012	0.0036	0.0081	0.0063	1.2
	500	1.3	0.25	0.020	0.033	0.0057	0.014	0.0085	0.96
	530	1.1	0.31	0.030	0.083	0.0102	0.022	0.015	0.77

ing the character of the interaction between components of the reaction mixture and between a component and the catalyst surface.

The experiments were carried out at $T = 460$–570°C, $P^0_{C_4H_{10}} = 0.08$–0.50 atm, and $P^0_{O_2} = 0.032$–0.18 atm.

$(N_2 + C_4H_{10})/(N_2 + O_2)$ and $(N_2 + O_2)/(N_2 + C_4H_{10})$ responses. The changes in the *iso*-C_4H_8 and CO_2 concentrations caused by the replacement of isobutane with oxygen, $(N_2 + C_4H_{10})/(N_2 + O_2)$, and by the reverse replacement, $(N_2 + O_2)/(N_2 + C_4H_{10})$, are shown in Figs. 5 and 6. In the $(N_2 + C_4H_{10})/(N_2 + O_2)$ response experiment with $NiMoO_4$, isobutene forms immediately, without any delay (Fig. 5a). This is probably due to the fact that isobutene, which was formed and adsorbed on the catalyst surface before air inlet, is desorbed upon this replacement. It is most likely that, immediately after atmospheric oxygen is admitted into the reactor, it begins to actively displace isobutene from the surface. This is indicated by the character of the CO_2 concentration changes in the same response run (Fig. 6a). The CO_2 appearance delay means that adsorbed oxygen is necessary for the deep oxidation products to be formed. In the $(N_2 + C_4H_{10})/(N_2 + O_2)$ response run, isobutene is no longer observed in the mixture 11 s after air admission (Fig. 5a), and this point in time almost coincides with the maximum CO_2 concentration time (Fig. 6a). Thus, it can be assumed that, in excess oxy-

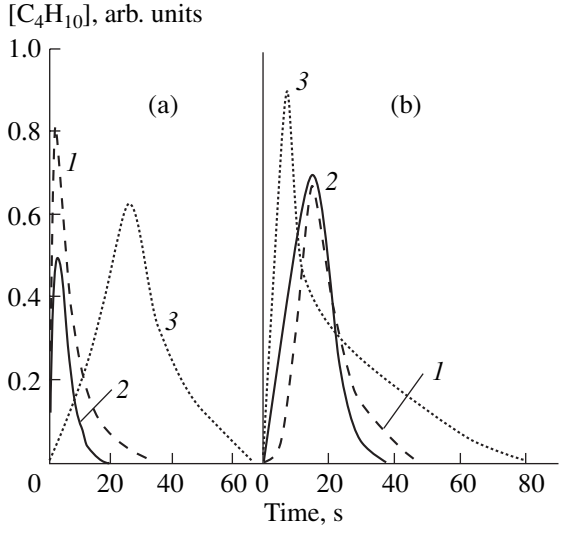

Fig. 5. Variation of the *iso*-C_4H_8 concentration in the (a) $(N_2 + C_4H_{10})/(N_2 + O_2)$ and (b) $(N_2 + O_2)/(N_2 + C_4H_{10})$ response runs with (*1*) $Co_{0.95}MoO_4$, (*2*) $NiMoO_4$, and (*3*) $MnMoO_4$ at $T = 530$°C and $P^0_{C_4H_{10}} = P^0_{O_2} = 0.2$ atm.

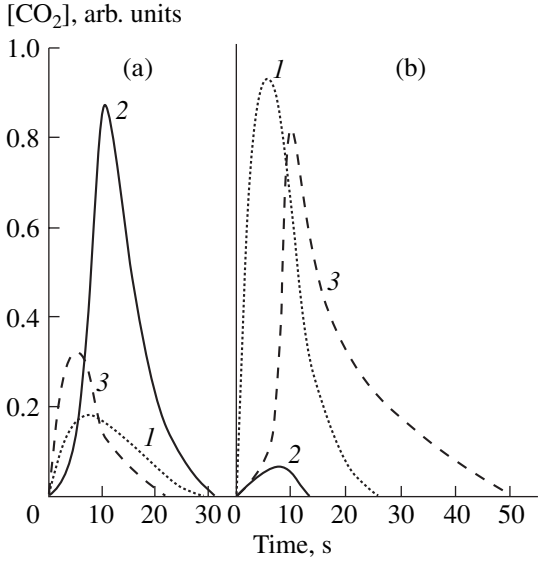

Fig. 6. Variation of the CO_2 concentration in the (a) $(N_2 + C_4H_{10})/(N_2 + O_2)$ and (b) $(N_2 + O_2)/(N_2 + C_4H_{10})$ response runs with (*1*) $Co_{0.95}MoO_4$, (*2*) $NiMoO_4$, and (*3*) $MnMoO_4$ at $T = 530$°C and $P^0_{C_4H_{10}} = P^0_{O_2} = 0.2$ atm.

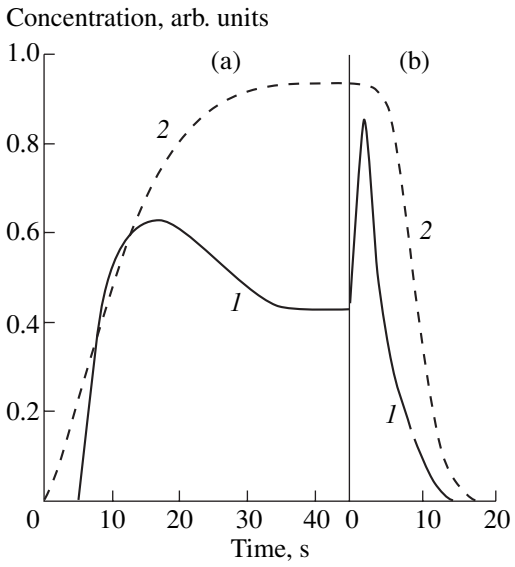

Fig. 7. Variation of the (*1*) *iso*-C_4H_8 and (*2*) CO_2 concentrations in the (a) $(N_2 + O_2)/(N_2 + O_2 + C_4H_{10})$ and (b) $(N_2 + O_2 + C_4H_{10})/(N_2 + O_2)$ response runs with $MnMoO_4$ at $T = 532$°C and $P^0_{C_4H_{10}}/P^0_{O_2} = 0.4$.

gen, all adsorbed products (olefin and, possibly, condensation products) are burnt. In the reverse response run $(N_2 + O_2)/(N_2 + C_4H_{10})$, the formation of *iso*-C_4H_8 is observed for approximately 28 s (Fig. 5b), a period of time much longer than in the $(N_2 + C_4H_{10})/(N_2 + O_2)$ response (Fig. 5a). Thus, isobutene is also formed in the absence of gaseous oxygen and virtually no olefin oxidation occurs. It is noteworthy that, in the absence of oxygen, the formation of *iso*-C_4H_8 on the molybdates examined ceases rapidly (Fig. 5b), indicating that the catalyst is inactive in simple dehydrogenation. After air admission (Fig. 5a), the catalyst is completely reactivated and the $(N_2 + O_2)/(N_2 + C_4H_{10})$ response run can be repeated. This cycling was performed multiply.

The different characters of the relaxation curves in Figs. 5 and 6 suggest that different forms of oxygen play the main role in the deep oxidation of hydrocarbons and in isobutane oxidative dehydrogenation. A low oxygen content of the reaction mixture leads to a low concentration of adsorbed oxygen, and this results in a considerable decrease in the proportion of CO_2 in the products and, at the same time, in a significant increase in the isobutene percentage. The latter effect is likely due to the lower oxidation rate of the adsorbed olefins.

No CO_2 delay was observed in the $(N_2 + C_4H_{10})/(N_2 + O_2)$ response run (Fig. 6a) with $Co_{0.95}MoO_4$, as distinct from $NiMoO_4$. In this case, the surface concentration of the hydrocarbons resulting from the interaction between isobutane and the catalyst surface (before air admission) is probably much lower than the same concentration in the case of nickel molybdate. The sharp increase of the CO_2 signal in the $(N_2 + O_2)/(N_2 + C_4H_{10})$ response run (Fig. 6b) is likely caused by the deep oxidation of the initial paraffin on the oxygen-saturated surface.

A distinctive feature of the isobutene curve in the $(N_2 + C_4H_{10})/(N_2 + O_2)$ response run with manganese molybdate is its symmetric shape (Fig. 5a). This shape indicates that, starting at the admission point, isobutene results mainly from isobutane oxidative dehydrogenation on the surface rather than from the displacement of isobutene with oxygen, contrary to the situation observed with $NiMoO_4$ or $Co_{0.95}MoO_4$. The fact that the constant CO_2 concentration is reached in a short time (~20 s) in the $(N_2 + C_4H_{10})/(N_2 + O_2)$ response run (Fig. 6a) indicates that the surface concentration of adsorbed hydrocarbons and coke before air admission is lower on $MnMoO_4$ than on $NiMoO_4$ or $Co_{0.95}MoO_4$. The duration of CO_2 formation on $MnMo_4$ is much longer for the $(N_2 + O_2)/(N_2 + C_4H_{10})$ response (Fig. 6b) than for the $(N_2 + C_4H_{10})/(N_2 + O_2)$ response (Fig. 6a) and is the longest in the series of catalysts examined. This is probably explained by the fact that the active oxygen concentration on the $MnMoO_4$ surface treated with oxygen is higher than the oxygen concentration on the $NiMoO_4$ or $Co_{0.95}MoO_4$ surface. The same is indicated by the run of the isobutene relaxation curve obtained in the $(N_2 + O_2)/(N_2 + C_4H_{10})$ response run with manganese molybdate (Fig. 5b).

$(N_2 + O_2)/(N_2 + O_2 + C_4H_{10})$ and $(N_2 + O_2 + C_4H_{10})/(N_2 + O_2)$ responses. The change in the *iso*-C_4H_8 concentration upon the replacement of air with the reaction mixture ($(N_2 + O_2)/(N_2 + O_2 +$ *iso*-C_4H_{10}) response) in the reaction on $Co_{0.95}MoO_4$ and $NiMoO_4$ was reported earlier [30]. The similar relaxation curves obtained for $MnMoO_4$ are presented in Fig. 7a. In all cases, the isobutene yield curve has a maximum. The higher the maximum, the larger the difference between the steady-state concentration of oxygen involved in isobutene formation and the oxygen concentration optimal for this process. The longest steady-state establishment time is observed in the response runs with manganese molybdate. The delay before the appearance of isobutene in the gas phase (Fig. 7a) is due to the fact that the high concentration of adsorbed oxygen prevents the release of C_4H_8.

In the reverse response run $(N_2 + O_2 +$ *iso*-$C_4H_{10})/(N_2 + O_2)$, when the reaction mixture is replaced with air, the isobutene concentration relaxation curve has a maximum for all catalysts (see [30] and Fig. 7b). Therefore, the steady-state surface concentration of oxygen involved in isobutene formation is below optimum at the given *iso*-C_4H_{10} concentration in the gas phase. This maximum is absent for cobalt molybdate below 520°C, indicating that the surface oxygen concentration is optimum for isobutene formation under these conditions.

The CO_2 concentration curves for the $(N_2 + O_2)/(N_2 + O_2 + C_4H_{10})$ response runs with $Co_{0.95}MoO_4$ and

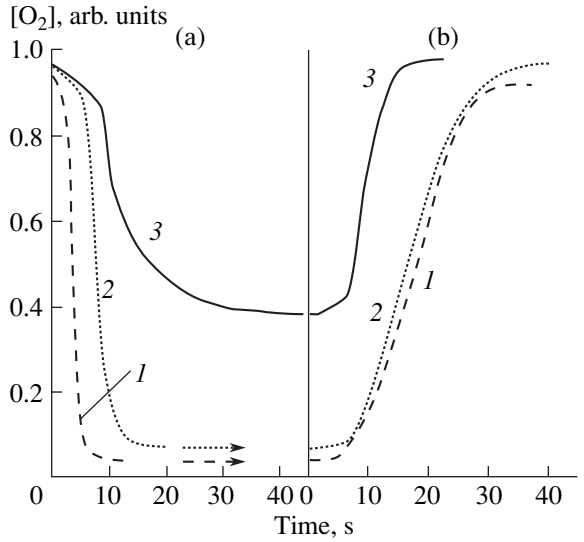

Fig. 8. Variation of the O_2 concentration in the (a) $(N_2 + O_2)/(N_2 + O_2 + C_4H_{10})$ and (b) $(N_2 + O_2 + C_4H_{10})/(N_2 + O_2)$ response runs with (*1*) $Co_{0.95}MoO_4$, (*2*) $NiMoO_4$, and (*3*) $MnMoO_4$ at 532°C. $P^0_{C_4H_{10}}/P^0_{O_2}$ = (*1*, *3*) 0.4 and (*2*) 1.0.

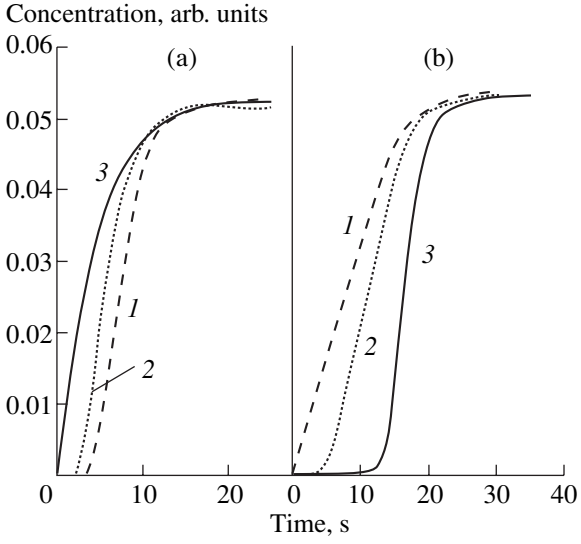

Fig. 9. $(N_2 + O_2)/N_2/(N_2 + O_2 + C_4H_{10})$ responses observed for $NiMoO_4$: (a) changes in the *iso*-C_4H_8 concentration for nitrogen purging times of (*1*) 10, (*2*) 20, and (*3*) 100 s; (b) changes in the CO_2 concentration for nitrogen purging times of (*1*) 0, (*2*) 30, and (*3*) 90 s; T = 500°C; $P^0_{C_4H_{10}}/P^0_{O_2}$ = 1.

$NiMoO_4$ [30] have a maximum, and the steady-state establishment time for these catalysts is approximately the same, being ~20 s. The presence of the extrema in the relaxation curves indicates that the formation of CO_2 is limited by an insufficient oxygen concentration on the surface at the given isobutane concentration in the mixture; i.e., the surface can be partially reduced under these reaction conditions. No maximum is observed for $MnMoO_4$ (Fig. 7a), and, hence, the surface of this catalyst undergoes no noticeable reduction under the steady-state conditions.

The presence of maxima in the CO_2 concentration curves for the $(N_2 + O_2 + C_4H_{10})/(N_2 + O_2)$ response runs involving $Co_{0.95}MoO_4$ and $NiMoO_4$ [30] is probably due to the buildup of adsorbed hydrocarbons and coke on the catalyst surface, which serve as a source of CO_2. For manganese molybdate (Fig. 7b), this relaxation curve has no maximum, indicating that the concentration of adsorbed hydrocarbons on the catalyst surface is much lower. The amount of adsorbed hydrocarbons (and coke) on all of the three catalysts can be estimated from the steady-state establishment time. This time is much longer (35 s) for $NiMoO_4$ than for $Co_{0.95}MoO_4$ (20 s) and $MnMoO_4$ (17 s).

The steady-state establishment time for oxygen in the $(N_2 + O_2)/(N_2 + O_2 + C_4H_{10})$ response runs with the cobalt and nickel catalysts is much shorter than on the same time for $MnMoO_4$ (Fig. 8a). Conversely, the reoxidation of the $MnMoO_4$ surface is more rapid than the reoxidation of $Co_{0.95}MoO_4$ or $NiMoO_4$ (Fig. 8b). The steady-state concentration of O_2 in the $(N_2 + O_2)/(N_2 + O_2 + C_4H_{10})$ response run with $NiMoO_4$ at $P^0_{O_2}/P^0_{C_4H_{10}} < 1$ is close to zero.

$(N_2 + O_2)/N_2/(N_2 + O_2 + C_4H_{10})$ responses. The roles of different surface oxygen species in isobutene formation and in deep oxidation were elucidated by measuring the responses of the reaction to changes in the feed composition, including intermediate purging of the system with nitrogen ($(N_2 + O_2)/N_2/(N_2 + O_2 + C_4H_{10})$ responses). By way of example, let us consider the relaxation curves of *iso*-C_4H_8 (Fig. 9a) and CO_2 (Fig. 9b) for $NiMoO_4$ and different nitrogen purging durations. As mentioned above, when no purging is used and, therefore, the catalyst surface is saturated with oxygen, the appearance of isobutene in the gas phase is somewhat delayed, whereas CO_2 appears in the gas phase without any delay. This is probably explained by the fact that most of the isobutane is initially converted into CO_x. Accordingly, isobutene either does not form or undergoes deep oxidation. As the purging time is extended, the isobutene appearance delay tends to zero and the CO_2 appearance delay increases.

These results indicate that, as the concentration of adsorbed oxygen decreases (as a result of nitrogen purging), the rate of deep oxidation decreases and the initial isobutene yield in the response run increases considerably. The formation of isobutene in the absence of adsorbed oxygen confirms the assumption that the lattice oxygen of the catalyst plays the main role in isobutene formation.

Stepped Mechanism of the Process

The fact that similar dependences of catalytic activity and *iso*-C_4H_8 and CO_2 selectivities on process conditions are observed for cobalt, nickel, and manganese molybdates, as well as the data obtained for these catalysts under unsteady-state conditions, suggest that isobutane oxidative dehydrogenation can be described in terms of the stepped mechanism proposed earlier for this reaction on cobalt and nickel molybdates [30]:

1. $C_4H_{10} + [O] = C_4H_8 + H_2O + [\ ]$,
2. $O_2 + [\ ] = O_2[\ ]$,
3. $O_2[\ ] + [\ ] = 2[O]$,
4. $O_2 + 2Z = 2ZO$,
5. $C_4H_{10} + 2ZO = C_4H_9OZ + OHZ$,
6. $2OHZ = H_2O + ZO + Z$,
7. $C_4H_9OZ + (8.5 + n)OZ = nCO_2 + (4 - n)CO + 4.5H_2O + (9.5 + n)Z$,
8. $C_4H_8 + Z = C_4H_8Z$,
9. $C_4H_8Z + ZO = C_4H_8OZ + Z$,
10. $C_4H_8OZ + (7 + n)OZ = nCO_2 + (4 - n)CO + 3.5H_2O + (8 + n)Z$,
11. $C_4H_{10} + Z = C_3H_6Z + CH_4$,
12. $C_3H_6Z = C_3H_6 + Z$.

Here, [ ] is an oxygen vacancy in the catalyst lattice, [O] is an occupied vacancy, Z is a free site on the catalyst surface, and ZO is chemisorbed oxygen.

According to this model, isobutene forms via a redox mechanism. The rate of step 3 exceeds the rates of steps 1 and 2, which determine the overall rate of oxidative dehydrogenation. The steady-state concentrations of oxygen and vacancies on the catalyst surface are maintained by the dynamic equilibrium of two processes, namely, the removal of oxygen as oxygen-containing reaction products in the reduction steps and the oxidation of vacancies by gaseous oxygen.

The reduction and oxidation rates are described, respectively, by the equations

$$r_{red} = k_{red} P_{C_4H_{10}} \theta \quad (6)$$

and

$$r_{ox} = k_{ox} P_{O_2} (1 - \theta), \quad (7)$$

where θ is the occupied fraction of oxygen vacancies.

In the steady state, these rates are equal and θ can be expressed as

$$\theta = \frac{k_{ox} P_{O_2}}{k_{ox} P_{O_2} + k_{red} P_{C_4H_{10}}}. \quad (8)$$

The isobutene formation rate equation will then take the form

$$r = k_{red} \frac{P_{O_2} P_{C_4H_{10}}}{P_{O_2} + \frac{k_{red}}{k_{ox}} P_{C_4H_{10}}}. \quad (9)$$

Oxygen-containing compounds are oxidized more rapidly and more readily than paraffins [33, 34], and, therefore, steps 5 and 9 are the slowest steps of deep oxidation and steps 4, 6–8, and 10 are fast or equilibrium. Step 11 is the slowest step in the formation of cracking products, and step 12 is assumed to be equilibrium.

If the reaction proceeds via adsorption on the uniformly heterogeneous catalyst surface, the rate of this step is described by the following equation [35]:

$$r = k \frac{\rho_1^{\gamma_1} \rho_2^{\gamma_2}}{(D)^{2\alpha}}, \quad (10)$$

where α is the linear correlation coefficient ($0 \le \alpha \le 1$; $\alpha = 0$ and $\alpha = 1$ formally correspond to the reaction taking place at a low and a high surface coverage, respectively), ρ_i is the volatility of the ith adsorbed reactants, and γ_i is the stoichiometric coefficients of the ith reactant. In the denominator, D is the sum of the adsorption equilibrium constants α_i multiplied by the volatility values ρ_i of the adsorption layer of the corresponding fragments. The calculated value of $\alpha = 0.5$ corresponds to intermediate coverages. When constructing the model, it was assumed that the main participants of the adsorption processes are oxygen, isobutene, and propene and that the adsorption constants of the last two compounds are similar.

It follows from Eqs. (1) and (9) that $k_I = k_{red}$ and $k_I = k_{red}/k_{ox}$. The larger k_{ox}, the smaller k_1. Thus, the efficiency of a catalyst is determined by the rate at which the oxygen vacancies in the lattice are occupied upon interaction with gaseous oxygen. When oxygen in the gas phase is deficient, the catalyst surface can be reduced. The reduced metal ions on the surface (for example, Co^0, Ni^+, and Mo^{5+}) are the sites of strong olefin adsorption and coke formation. Deactivation starts when the oxygen vacancies, which are the active sites of oxidative dehydrogenation, cannot be occupied. For $NiMoO_4$, the constant k_1 is the largest, and this explains the appearance of coke. Therefore, the $NiMoO_4$ catalyst can operate stably only at a high oxygen concentration in the gas phase (at O_2/*iso*-$C_4H_{10} \ge 1$). The $Co_{0.95}MoO_4$ and $MnMoO_4$ catalysts can operate stably at O_2/*iso*-$C_4H_{10} = 0.4$.

Excess oxygen in the gas phase increases the contribution from the oxidation reactions and reduces the olefin formation selectivity.

Effect of the Reaction Medium on the State of the Catalyst

Since, as shown above, the formation of isobutene on the catalysts includes redox steps taking place on the

surface, it is pertinent to study the effect of the reaction medium on the state of the catalyst preliminarily treated with isobutane or oxygen. The conception of the dependence of the catalytic properties of a heterogeneous catalyst on the chemical interaction between this catalyst and the components of the reaction system was formulated by Boreskov [36] and Rozovskii [37]. The relaxation method combined with mass spectrometric analysis is a tool for monitoring the state of the catalyst surface during the reaction [38]. Comparison between the relaxation curves obtained in the $(N_2 + C_4H_{10})/(N_2 + O_2 + C_4H_{10})$ and $(N_2 + O_2)/(N_2 + O_2 + C_4H_{10})$ response runs makes it possible to see how the system comes to its steady state for various initial states of the catalyst. In the former case, the catalyst is treated with a mixture of 30% isobutane and N_2; in the latter case, it is treated with air at 530°C for 30 s. The corresponding isobutene yield relaxation curves for $MnMoO_4$ are shown in Fig. 10. In both cases, the system reaches the same steady-state, but the olefin accumulation rate is lower and the steady-state establishment time is longer in the $(N_2 + C_4H_{10})/(N_2 + O_2 + C_4H_{10})$ response run than in the $(N_2 + O_2)/(N_2 + O_2 + C_4H_{10})$ response run. This implies that the reaction medium affects the state of the catalyst. The effects of the reaction medium are similar for cobalt and nickel molybdates. Thus, the preliminary treatment affects the state of the catalyst surface by initiating redox reactions.

Thus, this study has provided information concerning the processes that occur during isobutane oxidative dehydrogenation on $Co_{0.95}MoO_4$, $NiMoO_4$, and $MnMoO_4$. The formation of the major products in the presence of $MnMoO_4$ can be described by the kinetic equations set up earlier for the reactions taking place on cobalt and nickel molybdates. Nickel molybdate is the most active catalyst for both the formation and the total oxidation of isobutene. The high rate of deep oxidation of isobutene on $NiMoO_4$ is evidently due to the strength of its adsorption on this catalyst. As a consequence, the yield of *iso*-C_4H_8 is much lower on nickel molybdate than on $MnMoO_4$ or $CoMnO_4$.

The study of isobutane oxidative dehydrogenation by the response method showed that the highest and the lowest concentrations of reactive oxygen are observed on the manganese molybdate and nickel molybdate surfaces, respectively. Adsorbed oxygen plays the main role in the formation of carbon dioxide, and molybdate lattice oxygen is involved in the formation of isobutene.

In addition, it was demonstrated that the composition of the reaction medium exerts a considerable effect on the state of the catalyst surface. This is further evidence that the redox processes occurring on the catalyst surface play an important role in the oxidative dehydrogenation of isobutane.

Of the three molybdates considered, $Co_{0.95}MoO_4$ is the best catalyst for the oxidative dehydrogenation of isobutane.

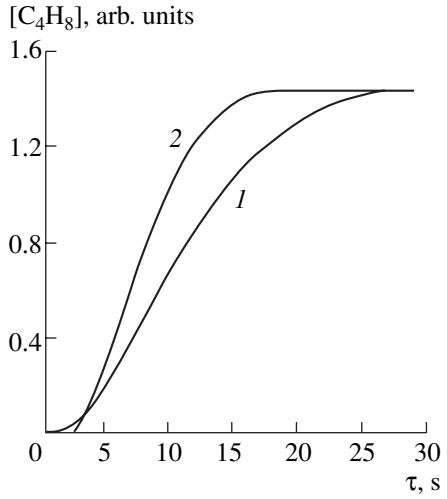

Fig. 10. Variation of the *iso*-C_4H_8 concentration in the (*1*) $(N_2 + C_4H_{10})/(O_2 + C_4H_{10})$ and (*2*) $(N_2 + O_2)/(N_2 + O_2 + C_4H_{10})$ response runs with $MnMoO_4$ at T = 530°C and $P^0_{C_4H_{10}}/P^0_{O_2} = 0.4$.

ACKNOWLEDGMENTS

This work was supported by the International Science Foundation, grant no. 96-1117.

REFERENCES

1. Buyevskaya, O.V. and Baerns, M., *Catal. Today*, 1998, vol. 42, no. 3, p. 315.
2. Cavani, F. and Trifiro, F., *Catal. Today*, 1999, vol. 51, nos. 3–4, p. 561.
3. Isagulyants, G.V., Belomestnykh, I.P., Forbek, G., and Perregaard, I., *Ross. Khim. Zh.*, 2000, vol. 44, no. 2, p. 69.
4. Bhasin, M.M., McCain, J.H., Vora, B.V., Imai, T., and Pujado, P.R., *Appl. Catal., A*, 2001, vol. 221, nos. 1–2, p. 397.
5. Kaddouri, A., Anouchinsky, R., Mazzocchia, C., Madeira, L.M., and Portela, M.F., *Catal. Today*, 1998, vol. 40, nos. 2–3, p. 201.
6. Rosso, R., Kaddouri, A., Fumagalli, D., Mazzocchia, C., Gronchi, P., and Centola, P., *Catal. Lett.*, 1998, vol. 55, no. 2, p. 93.
7. Madeira, L.M., Martin-Aranda, R.M., Maldonado-Hodar, F.J., Fierro, J.L.G., and Portela, M.F., *J. Catal.*, 1997, vol. 169, no. 2, p. 469.
8. Takita, Y., Sano, K., Kurosaki, K., Nishiguchi, H., Kawata, N., Ito, M., Akbay, T., and Ishihara, T., *Appl. Catal., A*, 1998, vol. 167, no. 1, p. 49.
9. Martin-Aranda, R.M., Portela, M.F., Madeira, L.M., Freire, F., and Oliveira, M., *Appl. Catal., A*, 1995, vol. 127, no. 1, p. 201.
10. Madeira, L.M., Maldonado-Hodar, F.J., Portela, M.F., Freire, F., Martin-Aranda, R.M., and Oliveira, M., *Appl. Catal., A*, 1996, vol. 135, no. 1, p. 137.

11. Madeira, L.M., Herrmann, J.M., Disdier, J., Portela, M.F., and Freire, F., *Appl. Catal., A*, 2002, vol. 235, no. 1, p. 1.
12. Madeira, L.M., Portela, M.F., Kaddouri, A., Mazzocchia, C., and Anouchinsky, R., *Catal. Today*, 1998, vol. 40, no. 2, p. 229.
13. Maldonado-Hodar, F.J., Palma Madeira, L.M., and Portela, M.F., *J. Catal.*, 1996, vol. 164, no. 2, p. 399.
14. Portela, M.F., Aranda, M.R., Madeira, M., Oliveira, M., Freire, F., Anouchinsky, R., Kaddouri, A., and Mazzocchia, C., *Chem. Commun.*, 1996, no. 6, p. 501.
15. Kaddouri, A., Mazzocchia, C., and Tempesti, E., *Appl. Catal., A*, 1998, vol. 169, no. 1, p. L3.
16. Cadus, L.E. and Ferretti, O., *Appl. Catal., A*, 2002, vol. 233, nos. 1–2, p. 239.
17. Tempesti, E., Kaddouri, A., and Mazzocchia, C., *Appl. Catal., A*, 1998, vol. 166, no. 2, p. L259.
18. Liu, Y., Wang, J., Zhou, G., Xian, Mo., Bi, Y., and Zhen, K., *React. Kinet. Catal. Lett.*, 2001, vol. 73, no. 2, p. 199.
19. Huang, Y., Cao, Y., Wang, G., and Corberan, V.C., *React. Kinet. Catal. Lett.*, 2002, vol. 75, no. 1, p. 31.
20. Cadus, L.E., Abello, M.C., Gomez, M.F., and Rivarola, J.B., *Ind. Eng. Chem. Res.*, 1996, vol. 35, no. 1, p. 14.
21. Yoon, Y.S., Ueda, W., and Morooka, Y., *Top. Catal.*, 1996, vol. 3, no. 2, p. 265.
22. Ueda, W., Lee, K.H., Yoon, Y.S., and Morooka, Y., *Catal. Today*, 1998, vol. 44, no. 2, p. 199.
23. Sautel, M., Thomas, G., Kaddouri, A., Anouchinsky, R., and Mazzocchia, C., *Appl. Catal., A*, 1997, vol. 155, no. 2, p. 217.
24. Rosso, R., Kaddouri, A., Mazzocchia, C., Anouchinsky, R., Gronchi, P., and Centola, P., *J. Mol. Catal. A: Chem.*, 1998, vol. 135, no. 2, p. 181.
25. Bennet, C.O., *Catal. Rev.—Sci. Eng.*, 1976, vol. 13, no. 2, p. 121.
26. Kobayashi, H. and Kobayashi, M., *Catal. Rev.—Sci. Eng.*, 1974, vol. 10, no. 2, p. 139.
27. Kobayashi, M., *Chem. Eng. Sci.*, 1982, vol. 37, no. 2, p. 393.
28. Pantazidis, A., Bucholz, S.A., Zanthoff, H.W., Schuurman, Y., and Mirodatos, C., *Catal. Today*, 1998, vol. 40, nos. 2–3, p. 207.
29. Creaser, D., Andersson, B., Hudgins, R.R., and Silveston, P.L., *Appl. Catal., A*, 1999, vol. 187, no. 1, p. 147.
30. Agafonov, Yu.A., Nekrasov, N.V., and Gaidai, N.A., *Kinet. Katal.*, 2001, vol. 42, no. 6, p. 899 [*Kinet. Catal.* (Engl. Transl.), vol. 42, no. 6, p. 821].
31. Mazzocchia, C., Renso, F., Aboumrad, C., and Thomas, G., *Solid State Ionics*, 1989, vol. 32, no. 2, p. 228.
32. Shub, F.S., Zyskin, A.G., Slin'ko, M.G., Snagovskii, Yu.S., and Temkin, M.I., *Kinet. Katal.*, 1981, vol. 22, no. 3, p. 744.
33. Nekrasov, N.V., Slinkin, A.A., Kucherov, A.V., Bragina, G.O., Katsman, E.A., and Kiperman, S.L., *Kinet. Katal.*, 1997, vol. 38, no. 1, p. 90 [*Kinet. Catal.* (Engl. Transl.), vol. 38, no. 1, p. 77].
34. Nekrasov, N.V., Botavina, M.A., Sergeeva, T.Yu., Dryakhlov, A.S., and Kiperman, S.L., *Kinet. Katal.*, 1998, vol. 39, no. 4, p. 543 [*Kinet. Catal.* (Engl. Transl.), vol. 39, no. 4, p. 502].
35. Kiperman, S.L., *Vvedenie v kinetiku geterogennykh kataliticheskikh reaktsii* (Introduction to the Kinetics of Heterogeneous Catalytic Reactions), Moscow: Nauka, 1964.
36. Boreskov, G.K., *Zh. Fiz. Khim.*, 1958, vol. 32, no. 12, p. 2739.
37. Rozovskii, A.Ya., *Katalizator i reaktsionnaya sreda* (Catalyst and Reaction Medium), Moscow: Nauka, 1988.
38. Ven'yaminov, S.A., *Mekhanizmy geterogenno-kataliticheskikh reaktsii okisleniya* (Mechanisms of Heterogeneous Catalytic Oxidations), Moscow: Nauka, 1993, p. 74.